Supplemental material to the manuscript:
"Coulomb bound states of strongly interacting photons"

M. F. Maghrebi,[1, *] M. J. Gullans,[1, *] P. Bienias,[2] S. Choi,[3] I. Martin,[4]
O. Firstenberg,[5] M. D. Lukin,[3] H. P. Büchler,[2] and A. V. Gorshkov[1]

[1]*Joint Quantum Institute and Joint Center for Quantum Information and Computer Science,*
NIST/University of Maryland, College Park, Maryland 20742, USA
[2]*Institute for Theoretical Physics III, University of Stuttgart, 70550 Stuttgart, Germany*
[3]*Physics Department, Harvard University, Cambridge, Massachusetts 02138, USA*
[4]*Materials Science Division, Argonne National Laboratory, Argonne, Illinois 60439, USA*
[5]*Department of Physics of Complex Systems, Weizmann Institute of Science, Rehovot 76100, Israel*

I. ADIABATIC ELIMINATION

In this section, we derive the Shrödinger equation (2) of the main text.

Upon adiabatic elimination of the intermediate state $|e\rangle$, the two-particle wave function is described by four components EE, ES, SE, and SS, each of which is a function of time and two spatial coordinates. We define $ES_\pm = (ES \pm SE)/2$ as the symmetric and antisymmetric combinations of the photon-Rydberg components. In the frequency domain, the Heisenberg equations can be cast as (see Refs. [S1]-[S2] for more details)

$$\omega EE = -ic\partial_R EE - \frac{2g^2}{\Delta}EE - \frac{2g\Omega}{\Delta}ES_+, \tag{S1}$$

$$\omega ES_+ = -\frac{ic}{2}\partial_R ES_+ - \frac{g^2+\Omega^2}{\Delta}ES_+$$
$$- ic\partial_r ES_- - \frac{g\Omega}{\Delta}(EE+SS), \tag{S2}$$

$$\omega ES_- = -\frac{ic}{2}\partial_R ES_- - \frac{g^2+\Omega^2}{\Delta}ES_- - ic\partial_r ES_+, \tag{S3}$$

$$\omega SS = -\frac{2\Omega^2}{\Delta}SS + V(r)SS - \frac{2g\Omega}{\Delta}ES_+, \tag{S4}$$

where ω is the frequency, $r = z - z'$ denotes the relative coordinate, and $R = (z + z')/2$ is the center of mass coordinate. For an infinitely long medium, one can work in Fourier space (relative to R) with the total momentum K. Defining $\psi(r) = ES_+(r)$, Eqs. (S1,S3,S4) yield, respectively,

$$EE = -\frac{2g\Omega}{\Delta}\frac{1}{\frac{2g^2}{\Delta}+\omega-cK}\psi, \tag{S5}$$

$$ES_- = \frac{-ic}{\frac{g^2+\Omega^2}{\Delta}+\omega-\frac{Kc}{2}}\partial_r\psi, \tag{S6}$$

$$SS = -\frac{2g\Omega}{\Delta}\mathcal{P}\left[\frac{\psi}{\frac{2\Omega^2}{\Delta}+\omega-V(r)}\right]+\alpha\delta[r-r_b(\omega)], \tag{S7}$$

with $\mathcal{P}$ denoting the principal part near the singularity at the blockade radius. The coefficient α is determined

by matching boundary conditions across the singularity. Inserting these expressions into Eq. (S2), we obtain a second-order differential equation for ψ as

$$-\frac{1}{m}\partial_r^2\psi + V_{\text{eff}}(r)\psi = E\psi, \tag{S8}$$

which is valid everywhere away from the blockade radius, i.e. for $|r| > r_b(\omega)$ and $|r| < r_b(\omega)$. The effective potential is given by

$$V_{\text{eff}}(r) = \frac{V(r)}{1 - V(r)/(\frac{2\Omega^2}{\Delta}+\omega)}, \tag{S9}$$

which, for $C_6\Delta > 0$, reduces to the effective potential in Eq. (2) of the main text. Defining the normalized units $\bar{\omega} = \omega\Delta/2\Omega^2$ and $\bar{K} = cK\Delta/2g^2$, the values of the energy and the mass take the form

$$E = \frac{2\Omega^2}{\Delta}(1+\bar{\omega})^2 \tag{S10}$$
$$\times\left[1 - \bar{K} + \frac{\Omega^2}{g^2}(1+2\bar{\omega}) - \frac{\Omega^2/g^2}{1-\bar{K}+\bar{\omega}\Omega^2/g^2} - \frac{1}{1+\bar{\omega}}\right],$$

$$m = \frac{g^4}{2\Omega^2\Delta c^2}\frac{1}{(1+\bar{\omega})^2}\left[1 - \bar{K} + \frac{\Omega^2}{g^2}(1+2\bar{\omega})\right]. \tag{S11}$$

It is worth pointing out that scattering theory techniques can be used to derive Eqs. (S8-S11) without adiabatically eliminating the excited state [S2] and to show their validity for a wide range of parameters. In particular, Eqs. (S8-S11) are an excellent approximation as long as $1 - \bar{K} \gtrsim \Omega^3/\Delta^3$ [S2], i.e., even for $\bar{K}$ close to 1.

The boundary conditions at the origin $[\psi'(0) = 0]$ and at infinity $[\psi(r \to \infty) = 0]$ are necessary to solve for ψ. Furthermore, the wavefunction should be continuous across the singularity at $r = r_b$. On the other hand, the discontinuity in its first derivative at $r = r_b$ determines the coefficient α, via Eqs. (S2,S3,S7), as

$$\alpha = -\frac{\Delta c/g\Omega}{(g^2+\Omega^2)/\Delta c + \omega/c - K/2}\partial_r\psi|_{r_b^-}^{r_b^+}. \tag{S12}$$

---

*These two authors contributed equally.

II. BOUNDARY CONDITION AT THE SINGULARITY

In this section, we show how to explicitly calculate $\partial_r \psi|_{r_b^-}^{r_b^+}$, and hence determine α via Eq. (S12), taking into account the boundary conditions at $r = 0$ and $r = \infty$. This is necessary for constructing the eigenbasis used in Fig. 2(b) of the main text.

Because of the singularity in V_{eff}, we find that α has both real and imaginary parts which can never simultaneously vanish. This implies that all eigenstates have a delta-function contribution. To show this, consider a small neighborhood near the singularity where Eq. (S8) takes the form

$$\frac{1}{U^2} \partial_x^2 \psi = \frac{1}{x-1} \psi, \tag{S13}$$

with $U \approx \frac{g^2 r_b(\omega)}{\sqrt{6}\Delta c} \sqrt{\frac{1-cK\Delta/2g^2}{1+\omega\Delta/2\Omega^2}}$ and $x = r/r_b(\omega)$. This equation is valid for $|x-1| \ll 1$ and has analytic solutions on both sides of the singularity in terms of first order Bessel functions

$$\psi_1^-(x) \approx \frac{\sqrt{1-x}}{U} J_1(2U\sqrt{1-x}), \tag{S14}$$

$$\psi_2^-(x) \approx -\frac{\pi\sqrt{1-x}}{U} Y_1(2U\sqrt{1-x}), \tag{S15}$$

$$\psi_1^+(x) \approx \frac{\sqrt{x-1}}{U} I_1(2U\sqrt{x-1}), \tag{S16}$$

$$\psi_2^+(x) \approx \frac{2\sqrt{x-1}}{U} K_1(2U\sqrt{x-1}), \tag{S17}$$

where $\mp$ refers to $x \lessgtr 1$, and the $\approx$ signs are meant to indicate that these equalities hold only for $|x-1| \ll 1$. The solutions ψ for all x are obtained by using Eq. (S8) to extend the above $\psi_{1,2}^\pm$ to all x. One then imposes the boundary conditions that ψ is symmetric about $x = 0$, i.e., $d\psi/dx(x = 0) = 0$, and $\psi(x) \to 0$ as $x \to \infty$. The solution for $x < 1$ can be written as

$$\psi(x) = c_1 \psi_1^-(x) + c_2 \psi_2^-(x), \tag{S18}$$

where c_1 and c_2 are determined by the boundary condition at $x = 0$. For $x > 1$, one can show that the choice of ψ_2^+ in terms of the Bessel function of the second kind K_1 near the singularity guarantees that, away from the singularity where Eqs. (S15)-(S17) are no longer valid, ψ_2^+ decays exponentially for large values of x, while ψ_1^+ grows exponentially. Imposing the boundary condition that ψ vanishes at infinity implies $\psi(x) \propto \psi_2^+(x)$, while the continuity of $\psi(x)$ at $x = 1$ gives the result

$$\psi(x) = \begin{cases} c_1 \psi_1^-(x) + c_2 \psi_2^-(x), & x < 1, \\ c_2 \psi_2^+(x), & x > 1. \end{cases} \tag{S19}$$

The contribution of $\psi_1^\pm$ to $\partial_x \psi|_{1^-}^{1^+}$ is c_1. However, calculating the contribution of $\psi_2^\pm$ to $\partial_x \psi|_{1^-}^{1^+}$ requires more care because, near the singularity, $\partial_x \psi_2^\pm \sim \log(1-x)$. To

help resolve this, we examine the solutions in the presence of an infinitesimal decay rate γ' from the Rydberg state. In this case, near the singularity, the effective Schrödinger equation takes the form

$$\frac{1}{U^2} \partial_x^2 \psi = \frac{1}{x-1+i\epsilon} \psi, \tag{S20}$$

where $\epsilon = \gamma'/(\omega + 2\Omega^2/\Delta)$. Using the relation

$$\lim_{\epsilon \to 0} \frac{1}{x-1+i\epsilon} = \mathcal{P}\left(\frac{1}{x-1}\right) - i\pi\delta(x-1), \tag{S21}$$

and integrating Eq. (S20) across the singularity suggests a contribution to $\partial_x \psi|_{1^-}^{1^+}$ equal to $-i\pi\, U^2 \psi(1) = -i\pi c_2$. Combining this result with the c_1 contribution gives

$$\alpha = -\frac{\Delta c/g\Omega r_b}{(g^2 + \Omega^2)/\Delta c + \omega/c - K/2}(c_1 - i\pi\, c_2). \tag{S22}$$

With this final result, we can construct the complete set of states used in making Fig. 2(b) of the main text. First, we solve numerically for ψ inside the blockade radius. We then find c_1 and c_2 by matching these numerical solutions, in a region near the singularity, to the analytic solutions in Eqs. (S14)-(S15). To check the arguments presented above, we have also verified numerically that when the imaginary component to α is neglected the resulting solutions do not form an orthonormal basis, while, when the imaginary term is included, the solutions are consistent with an orthonormal basis.

Since $c_{1,2}$ can be assumed to be real numbers, which cannot both vanish, it is clear that all eigenstates have the delta-function contribution. This is consistent with the fact that, for $g = 0$, the continuum is composed of Rydberg molecule states. For finite g, these states become dressed with the photons, but do not lose their character as atomic bound states. The eigenstates linked to the Coulomb states have the special property that $c_2 = U^2 \psi(1) = 0$.

From this solution, we can also determine the behavior of the eigenstates as the interaction strength $U \to \infty$. At the singularity, $\psi(1) = c_2/U^2$, which implies that, as U increases, $\psi(1) \to 0$ and all solutions satisfy the same boundary condition at the singularity. Additionally, in this limit $\alpha \to 0$, which implies that the states confined inside the Rydberg blockade completely decouple from the continuum of Rydberg molecule states (i.e., the delta functions). In this limit, the Coulomb states (without the delta function) therefore become exact eigenstates and would show zero spectral width in Fig. 2(b) of the main text. This is again analogous to the leaky box discussed in the main text, where, as the box becomes infinitely deep, the eigenstates inside the well become decoupled from the continuum of momentum states that live outside the box.

III. NUMERICAL METHODS

In this section, we describe the numerical methods used to obtain Fig. 3 of the main text.

We include the decay rate 2γ of the intermediate state by adding an imaginary component to Δ. Decay (with rate $2\gamma'$) of the Rydberg state requires adding the term $-i\gamma' \int dz\, S^\dagger(z)S(z)$ to the Hamiltonian.

Within the two-excitation subspace, H can be split into a kinetic term T that describes the propagation of photons and a part W that is diagonalizable in real space, that includes the Rydberg-Rydberg interaction, decay, and coupling to the quantum and classical light fields. We can then find the time-evolution of the wavefunction by a Trotter decomposition, whereby we split the propagator into two parts which are separably diagonalizable in momentum (T) and real-space (W)

$$e^{-iH\tau} \approx e^{-iT\tau/2}e^{-iW\tau}e^{-iT\tau/2} + O([W,T]\,\tau^2). \quad \text{(S23)}$$

In our case, $\mathcal{E}$ has a linear dispersion, which implies that propagation with T corresponds to a uniform shift in real-space of the $\mathcal{E}$-components of the wavefunction, while $e^{-iW\tau}$ can be found exactly for each point in space. Using these solutions, we can construct the long-time-evolution by stepwise application of Eq. (S23) for small τ.

For the experimental parameters in Fig. 3 of the main text, the group velocity $v_g/c \approx \Omega^2/g^2 \approx 10^{-8}$, which implies that there is a large separation of time scales between the light propagation and the atomic dynamics. Just increasing the time step cannot overcome this because the error term in the Trotter decomposition becomes very large. This problem can, however, be overcome by bringing the time scales closer together through the scaling transformation $z \to \zeta z$, $g \to g/\sqrt{\zeta}$, and $r_b \to \zeta r_b$. One can see from Eqs. (S10-S11) that the dynamics are invariant under this transformation provided $v_g\zeta/c \ll (1-\bar{K})^2$. To obtain Fig. 3 of the main text, we use $\zeta = 1.2 \times 10^7$, which satisfies this condition.

The observation of Coulomb states requires large interaction strengths (equivalently atomic densities). This in turn requires a fine numerical mesh for the wavefunction, which makes the simulations very time consuming. However, since the Coulomb states are confined to a region on the order of the blockade radius we can force the wavefunction to be zero outside a region on the order of a few blockade radii. This significantly reduces the required memory and simulation time. We have verified that our numerical results are insensitive to this cutoff.

Finally, H is an effective Hamiltonian obtained after adiabatically eliminating the intermediate state $|e\rangle$. We have also verified numerically that our results hold when state $|e\rangle$ is explicitly included in the simulations.

IV. CONDITION FOR REPULSIVE CORE

In this section, we establish the parameter regime when the effective energy $E < V_{\text{eff}}(0)$. In this case, the two-
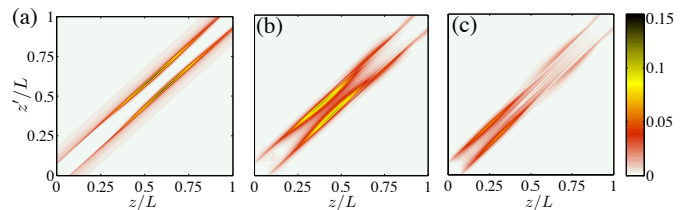
FIG. S1: Time evolution of the $n = 1$ Coulomb state as in Fig. 3 of the main text, except here we take a much larger value of $g^2 r_b/c\Delta$ and much smaller decay rates to verify that our analytical theory accurately describes the Coulomb states. The initial condition for EE, ES, and SE is chosen to be zero, while SS is chosen to be given by Eq. (S24) with $\sigma = \Omega^2/2\Delta$ and $n = 1$. The $|EE|$ component is shown (a) shortly after $t = 0$ at $tv_g/L = 10^{-4}$ and at later times (b) $tv_g/L = 3 \cdot 10^{-3}$ and (c) $tv_g/L = 6 \cdot 10^{-3}$. Here L is the length of the medium, and we took $g^2 r_b/c\Delta = 40$, $\Omega/g = 0.05$, $L/r_b = 14$, $\Omega/\Delta = 0.25$, $\gamma/\Delta = 0.05$, and $\gamma' = 0$. For these parameters, in contrast to those of Fig. 3 in the main text, the EE component of the Coulomb state is localized near the blockade radius.

photon state feels a repulsive core and becomes peaked near the points $\pm r_b$. From Eq. (S10) and Eq. (S11) we can see that, for $\Omega^2/g^2 \ll 1$, we can rewrite

$$E - V_{\text{eff}}(0) \approx \frac{2\Omega^2}{\Delta} \frac{(1+\bar{\omega})^2}{1-\bar{K}}\left[(1-\bar{K})^2 - \Omega^2/g^2\right],$$

which becomes negative when $1 - \bar{K} < \Omega/g$. Note that, in order for the adiabatic elimination to be valid near $\bar{K} = 1$, we also require $1 - \bar{K} \gg \Omega^3/\Delta^3$ [S2]. This sets the constraints $\Omega/g > 1 - \bar{K} \gg \Omega^3/\Delta^3$, in order to have a repulsive core, which can be easily satisfied.

In Fig. S1 we show the resulting backward propagating state under the same preparation procedure as described in the main text and Fig. 3, except in this case we took smaller decay rates, a larger value of $g^2 r_b/c\Delta$ and a much larger control field intensity. In particular, the Coulomb state we prepared had $1 - \bar{K} \approx 0.02$ and $\Omega/g = 0.05$. The double peaked structure is clearly visible, consistent with the presence of the repulsive core for this bound state. The possibility of such tight localization of Coulomb bound states around $r = \pm r_b$ contrasts with the bound states found when $C_6\Delta < 0$. The latter are centered at $r = 0$ and have width $\gtrsim r_b$ [S2, S3].

V. GROUP VELOCITY OF COULOMB STATES

In this section, we compare the group velocity predicted by the WKB treatment in the main text with numerical simulations for $n = 1$, 2, and 3. To construct the Coulomb wavepacket, we first choose a narrow range of frequencies around $\omega = 0$ and, for every ω, we find $K_n(\omega)$ from Eq. (4) in the main text, which gives us an expression for $p_n(r,\omega)$. The initial state has $EE = ES = SE = 0$ with SS given by the variational
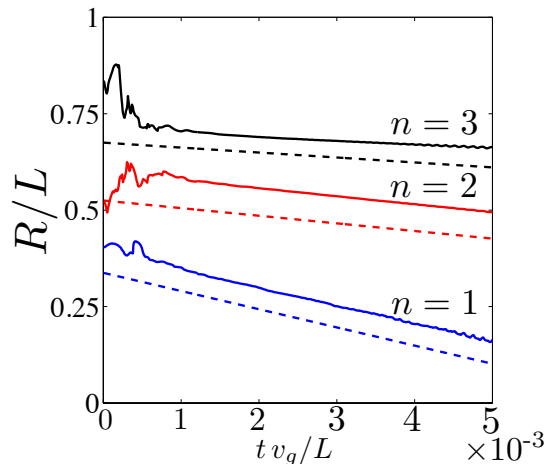
FIG. S2: Time evolution of the average center of mass position of the Coulomb wave packets with parameters as in Fig. S1. The initial state is given by Eq. (S24). The horizontal axis is propagation time in units of L/v_g, while the vertical axis is defined as the average over $r < r_b$ of the position of the peak values of the EE-component of the wavefunction, where, at each r, the peak value is defined with respect to R. The $n = 2$ and 3 curves are shifted vertically for visibility. The dashed lines are the prediction for the group velocity from Eq. (5) in the main text and are also plotted with a shift relative to solid curves for visibility. The extracted slope from the linear region of the simulations agrees with the predicted group velocity to within a few percent for each n.

wavefunction

$$SS_n(r, R) = \mathcal{N} \int d\omega \, e^{iK_n(\omega)R - \omega^2/\sigma^2} \frac{1}{1 - [r_b(\omega)/r]^6}$$
$$\times \left[(-1)^n - \cos \int_0^r p_n(r, \omega) \right] \Theta[r - r_b(\omega)],$$
$$(S24)$$

which vanishes at $r_b(\omega)$ for every ω. Here $\mathcal{N}$ is a normalization constant, σ is the width of the wavepacket, and Θ is the Heaviside step function.

The results are shown in Fig. 3 of the main text and in Figs. S1-S2. Fig. 3 of the main text and Fig. S1 show snapshots of the backward-propagating $n = 1$ wavefunction. While Fig. 3 of the main text uses experimentally realistic parameters, Fig. S1 assumes larger $g^2 r_b/c\Delta$ and smaller decay rates to verify that our analytical theory describes the Coulomb states accurately. Indeed, in Fig. S2, which uses the parameters of Fig. S1, we see excellent agreement between the numerical simulations and the predicted group velocity. For each n, the extracted slope in the linear region agrees with the predicted value to within a few percent. For $n = 1$, 2 and 3, the group velocity of the Coulomb states for these parameters is approximately $-50 \cdot v_g$, $-20 \cdot v_g$ and $-10 \cdot v_g$, respectively.

VI. NON-NEGATIVITY OF GROUP VELOCITY

In this section, we show that the group velocity in a system with, possibly interacting, right-going modes cannot be negative for normalizable eigenstates. Let us write the Schrödinger equation as

$$H_K|\Psi_K\rangle = \omega_K|\Psi_K\rangle, \qquad (S25)$$

where we have made explicit the dependence on some parameter K, which will be identified later as the total momentum of two particles. One can then see that

$$\partial_K \omega_K = \langle \Psi_K|\partial_K H_K|\Psi_K\rangle + \omega_K \partial_K \langle \Psi_K|\Psi_K\rangle$$
$$= \langle \Psi_K|\partial_K H_K|\Psi_K\rangle, \qquad (S26)$$

where the second term in the first line vanishes for a normalized state $\langle \Psi_K|\Psi_K\rangle = 1$. This result is known as the Hellmann-Feynman theorem.

For our system, we can cast the Hamiltonian in the two-particle sector in the basis defined by $(EE \ ES_+ \ ES_- \ SS)^T$. (The generalization to the case where $|e\rangle$ is not adiabatically eliminated is straightforward.) Identifying K with the total momentum, from Eqs. (S1-S4), we have

$$\partial_K H_K = \delta(r - r') \begin{pmatrix} c & 0 & 0 & 0 \\ 0 & c/2 & 0 & 0 \\ 0 & 0 & 0 & 0 \\ 0 & 0 & 0 & 0 \end{pmatrix}, \qquad (S27)$$

which is a nonnegative matrix acting on the Hilbert space associated with the relative coordinate r (the center-of-mass plane wave, although not normalizable, does not enter the argument). Therefore, the group velocity $v_g = \partial \omega_K/\partial K$ given by Eq. (S26) cannot be negative for any eigenstate whose relative-coordinate wavefunction is normalizable.

VII. EXPERIMENTAL CONSIDERATIONS

In this section, we point out several conditions necessary for the treatment of the medium as a one-dimensional continuum of stationary atoms [Eq. (1) in the main text] and hence for the experimental observation of Coulomb states. We also discuss the effects of finite decay rate $2\gamma'$ of the Rydberg state.

First, the delta functions appearing in the underlying exact eigenstates should be consistent with the treatment of atoms as a continuous medium. This requires $\rho(\pi w^2)w_\delta \gg 1$, where ρ is the atomic density, w is the beam waist, and $w_\delta \sim |dr_b(\omega)/d\omega|/\tau$ is the effective width of the delta function due to the uncertainty in ω coming from the finite duration of an experiment τ, which is in turn limited by the lifetime of the Coulomb states [$\sim \Delta/2\Omega^2$ from Fig. 2(b) in the main text]. Recent experiments achieved a density of $\rho = 2 \times 10^{12}$ cm^{-3} with a beam waist of $w = 4.5$ μm, corresponding to

$g/2\pi \approx 4$ GHz [S3]. We will use below the parameters of Fig. 3 in the main text, where $g/2\pi = 17$ GHz, so we will take $w = 4.5$ μm and $\rho = 3.6 \times 10^{13}$ cm^{-3}. Taking $\tau = t_f$, we then find $w_\delta \approx 0.2$ μm and $\rho(\pi w^2)w_\delta \approx 200$.

Second, two atoms initially r_b away from each other should not change their distance by more than w_δ if they are displaced transversely by w. This leads to the condition $w < \sqrt{w_\delta r_b}$, which is nearly satisfied, and can be more strictly satisfied by changing the center frequency of the wavepacket to increase $r_b(\omega)$.

Third, the force on a pair of Rydberg atoms r_b apart and their thermal velocity must both induce motion less than w_δ over time τ, leading to the conditions $6C_6\tau^2/(mr_b^7), \tau\sqrt{k_B T/m} < w_\delta$. Using the mass m of ^{87}Rb and temperature $T = 35$ μK [S4], the first condition is satisfied (0.07 μm < 0.2 μm). The second condition can be satisfied by using a sufficiently high control field intensity.

Finally, we note that the decay rate $2\gamma'$ of the Rydberg state can be ignored provided it is much smaller than the inverse time τ^{-1} of the experiment. In the supplement (Figs. S1 and S2), γ' was taken to be zero. Since the duration of the experiment in Fig. S1 is $\tau = 6 \cdot 10^{-3}L/v_g = 2.7/\gamma$, γ' can be ignored provided $2\gamma' \ll \gamma/2.7$, which is satisfied in existing experimental systems [S4].

In the main text (Fig. 3), the duration of the experiment is $\tau = 5.5\Delta/\Omega^2 = 0.7/(2\gamma')$, i.e. it is shorter than $1/(2\gamma')$ but not much shorter. (While optimistic, the chosen value of γ' is realistic as it is only an order of magnitude smaller than the values already demonstrated experimentally [S4].) The resulting non-negligible γ' decay, along with γ-induced decay, contributes to the factor of 0.05 drop in color scale between Fig. 3(b) and Fig. 3(d) of the main text. The fact that we still see the negative group velocity and the expected shape of the bound state in the figure means that these features are robust even in the presence of non-negligible γ' decay [5].

[S1] A. V. Gorshkov, J. Otterbach, M. Fleischhauer, T. Pohl, and M. D. Lukin, Phys. Rev. Lett. **107**, 133602 (2011).
[S2] P. Bienias, S. Choi, O. Firstenberg, M. F. Maghrebi, M. Gullans, M. D. Lukin, A. V. Gorshkov, and H. P. Büchler, Phys. Rev. A **90**, 053804 (2014).
[S3] O. Firstenberg, T. Peyronel, Q.-Y. Liang, A. V. Gorshkov, M. D. Lukin, and V. Vuletic, Nature (London) **502**, 71 (2013).
[S4] T. Peyronel, O. Firstenberg, Q.-Y. Liang, S. Hofferberth, A. V. Gorshkov, T. Pohl, M. D. Lukin, and V. Vuletic, Nature (London) **488**, 57 (2012).
[5] It is worth noting that we can map a problem with finite γ' to a problem with vanishing γ' by making the following substitution in the former: $\omega \to \omega - i2\gamma'$ and $K \to K - i2\gamma'/c$.